can be achieved only for an ∞-atomic gas, it behaves as a singularity during the solution procedure and the graphs of Fig. 1 become undefined at this value. However, it can be seen from Fig. 1 that as γ_1 and γ_2 decrease to 1, points B and C move toward A. From this it can be inferred that in the limiting case of $\gamma \rightarrow 1$, B and C will be located at (∞, ∞). Similarly, D, G, and H will be located at (∞, ∞) and E, F, and I will be located at (1, 1).

Under the prestated constraint on H_1/H_2, the region of flow that can be analyzed with the method of characteristics is *CBOED* in Fig. 1. On violation of this constraint expansion waves from stream 2 are transmitted into stream 1 upstream of the reflected oblique shock, curving it and increasing its strength. As a result many streams of continuously varying Mach number are formed downstream of the reflected oblique shock, which may be subsonic. This phenomenon introduces a demarcation line (*KL*, for $H_1/H_2 = 1$ and $\gamma_1 = \gamma_2 = 1.4$) in the region *CBOED* and reduces the domain of applicability of analysis (to *CBKLD*). The exact location and shape of this line depends on H_1/H_2, γ_1, and γ_2. In the region *KOEL*, $X_{SS} > X_{ES}$ and in *CBKLD*, $X_{SS} < X_{ES}$. Though *CBKLD* appears to be an open region from the upper end *CD*, it probably is not so. For certain inlet Mach number combinations an upper limit might also be imposed by formation of an oblique shock in stream 2 from the point of intersection of the reflected oblique shock and the slip stream. The location and shape of this line will also be functions of the tunnel geometry and inlet flow parameters.

Shape of the Slip Stream

Computed slip-stream shapes are shown in Fig. 2. The discontinuity in the slope of the slip stream at the point of intersection by the reflected oblique shock is clearly marked. Furthermore, for a given value of M_2, the change in the abscissa of the point of intersection of the reflected oblique shock and the slip stream is negligibly small. This point houses the first major maxima of the shape. The ordinates of the maxima increase as M_1 increases and have an upper bound of ≈ 0.45 before the occurrence of the secondary shock in stream 2 upstream of the following minima. Downstream of the maxima, curvature of the slip stream slowly increases, and a point of inflection occurs just upstream of the first minima. The abscissa of the minima is almost twice that of the maxima. The probability of occurrence of a shock in the upstream neighbourhood of the minima is very high, as is indicated by the kinks in the slip-stream shape at this location for high values of M_1. The kinks indicate actual formation of Mach disk or shock-like compression front in stream 2 because of the intersection of Mach waves of the same family. Increase in the size of the kink with an increase in M_1 indicates its proportionality with the strength of the secondary shock. The absence of a kink at this location does not imply the complete absence of shocks. In fact, it indicates the formation of shocks in stream 1 downstream of the minima rather than in stream 2. It should also be observed that the slip stream flattens out as M_2 increases. The maxima and the minima move forward on the abscissa, and the ordinates of these points decrease. Still, the ratio of the abscissa of these points remains almost the same.

All the computations were performed in single precision to an accuracy of 10^{-5} except in Fig. 1 where it was reduced to 10^{-2} in M_1 and M_2 to save computer time. For computation of the slip-stream shape, the angular separation between consecutive characteristics was taken to be 1 deg.

Discussion

Though the methodology presented in the preceding sections is promising in that it can reveal vital structural information about a flow space, it should be used with caution since assumptions of inviscid and planar flowfield break down in most practical situations. Viscosity leads to dissipation in the strength of shock waves, changing the analysis drastically. Still, with appropriate modifications in the numerical scheme the methodology outlined here can be adopted in most flow situations. It is expected that even after adaptations are incorporated to take care of the viscosity, three-dimensionality, and mixing in the flowfield, the philosophy, efficiency, and use of the analysis methodology presented here would remain unaltered.

The slip stream has been considered as an infinitely thin interface, which is acceptable as a first approximation. In actual flowfields the slip stream is considerably thick because of mixing, and thickness increases as one goes downstream. In these cases the infinitely thin interface may (perhaps) be taken to be some mean line of the slip stream.

References

[1]Otis, D. R., "Choking and Mixing of Two Compressible Fluid Streams," *Transactions of the ASME, Journal of Fluids Engineering*, Vol. 98, No. 2, 1976, pp. 311–317.

[2]Papamoschou, D., "Diffuser Performance of Two-Stream Supersonic Wind Tunnels," *AIAA Journal*, Vol. 27, No. 8, 1989, pp. 1124–1127.

[3]Shapiro, A. H., *The Dynamics and Thermodynamics of Compressible Fluid Flow*, Vol. 1, Wiley, New York, 1953; Vol. 2, Ronald Press, New York, 1954.

Suppression of Vortex Asymmetry and Side Force on a Circular Cone

A. Asghar,* W. H. Stahl,† and M. Mahmood*
King Fahd University of Petroleum and Minerals, Dhahran 31261, Saudi Arabia

Introduction

It is a well-documented fact that the flow about a slender pointed body of revolution at zero yaw becomes asymmetric at some high angle of attack; e.g., see Ref. 1. The initially symmetric vortex pair on the lee side rearranges into an asymmetric configuration with the asymmetry starting either at the tail of a long afterbody or at the tip of a slender, pointed nose. This asymmetric flow leads to a side force acting on the body. A similar phenomenon of an initially symmetrical vortex pair becoming asymmetric has been observed long ago on a circular, two-dimensional cylinder set into motion impulsively in a fluid initially at rest.[2] This flow was studied theoretically by Foeppl.[3] He investigated the stability of the symmetrical vortex pair with respect to small, symmetric and antisymmetric displacements and found that the symmetrical vortex pair is stable for symmetric but unstable for antisymmetric disturbances. This result suggested that a "fin" between the vortices would lead to stable, symmetric flow. These considerations were carried over by means of unsteady-flow analogy to the three-dimensional vortex flow behind the corresponding inclined cylinder and qualitatively to the inclined cone.[4] The effect of such a fin on the flow past a slender cone was studied by means of flow visualization in a water tunnel at a low value of Reynolds number and in a low-speed wind tunnel at about 10 times the value of *Re*. The fin largely suppressed vortex-flow asymmetry; therefore, a quantitative investigation of the surface pressures and forces on the cone without and with fin was carried out.

Results were reported by Ng,[5] concurrently with Stahl's first results,[4] on such a fin on a nose suppressing vortex asymmetry. Various other methods have been found to be effective in reducing or suppressing vortex-flow asymmetry; e.g., see Ref. 1.

Experimental Setup and Techniques

The wind tunnel that we used at King Fahd University of Petroleum and Minerals (KFUPM) is of the partially open return type with a closed horizontal test section of 0.8 m × 1.1 m and length of

Received July 31, 1993; presented as Paper 94-0508 at the AIAA 32nd Aerospace Sciences Meeting, Reno, NV, Jan. 10–13, 1994; revision received April 18, 1994; accepted for publication May 3, 1994.

*Lecturer, Department of Mechanical Engineering.

†Adjunct Professor, Department of Mechanical Engineering. Senior Member AIAA.

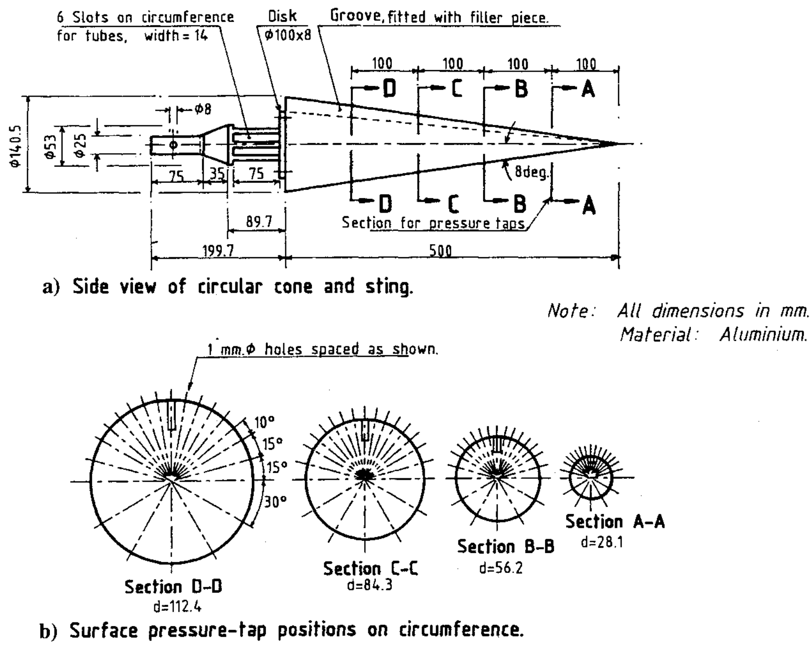

Fig. 1 Surface-pressure measurement model and mounting.

3 m. Maximum freestream velocity is $U_\infty = 35$ m/s. The basic circular cone had a semi-apex angle $\delta_N = 8$ deg, length $L = 500$ mm, and base diameter $D = 140.5$ mm. To this cone could be added a vertical flat-plate fin extending from the tip to the base, with its outer edge on a ray through the cone apex. Fin height above the cone surface was $H_f/R_{\text{sec}} = 1.0$ (R_{sec} denotes the sectional radius of cone). Pressure taps ($\phi = 1$ mm) were arranged on the circumference at four axial sections at distances from the apex $X/L = 0.2$, 0.4, 0.6, and 0.8, respectively; see Fig. 1. A groove of 4-mm width for application of the fin along the uppermost lee-side generator was closed by a filler plate when the fin was not used. The hollow cone was made of two symmetrical vertical shells. The surface was left in the machined condition; i.e., no paint was applied. The pressure taps were connected by means of plastic tubes (1.5-mm inner diameter) to the manometers outside the test section. The model was supported at the base on a sting through which the plastic tubes came out (see Fig. 1) and kept approximately in the middle of the test section for all tests. The fin was also equipped with surface pressure taps on both sides, at the same axial sections as the taps on the cone.

The pressure measurements were performed, at one fixed roll angle, at angles of attack $\alpha = 15$, 17, 20, 25, 30, and 35 deg and nominally zero yaw ($\beta \leq 0.2$ deg) at $Re_D = 1.42 \times 10^5$ (formed with base diameter D) using Betz-type manometers. The circumferential pressure distributions on the basic cone were subsequently integrated to give sectional side and normal forces. Full results are reported in Ref. 6.

Results and Discussions

The value of the Reynolds number of our tests suggests that a laminar boundary layer is separating from the cone.[1] However, the flow passes over pressure taps and various covered holes and gaps, and it is known that pressure taps can act like tripping wires, leading to premature transition of the laminar boundary layer. Surface oil-flow visualizations did not provide conclusive results in this respect.

The circumferential pressure distributions on the cone without fin show onset of distinct asymmetry, with respect to the incidence plane, at $\alpha = 17$ deg, and the degree of asymmetry is becoming larger with increasing incidence. When the fin is attached along the cone's leeward generator, the circumferential pressure distributions become practically symmetrical, clearly revealing the effect of the fin in largely suppressing the large vortex-flow asymmetry present on the basic cone. This is shown, in an exemplary way, in Fig. 2 by the pressure distributions, without and with fin, at $\alpha = 35$ deg at section C. However, with the fin attached, there is a small degree of asymmetry left; in general, with higher suction on the starboard side, and more expressed at the foremost section, A. This is probably attributable to the fact, that a small lateral dislocation of the fin near the tip sets up a relatively large asymmetry in the model geometry.

There were also pressure taps on each side of the fin aligned with the measuring sections of the cone. At the three axial sections B, C, and D, the suction along the height of the fin is distributed fairly symmetrically on both sides. In section A, due to some clogged pressure taps, meaningful comparisons were not possible.

The circumferential pressure distributions were subsequently integrated to obtain the sectional side and normal force coefficients, C_y and C_n, respectively (with forces based on dynamic pressure and sectional diameter), at each of the four axial measuring sections. Sectional side forces on the cone, without fin, distinctly appear at $\alpha = 17$ deg, due to the clear asymmetry in the pressure distribution. With increase in angle of attack, the leeside vortex flow as well as the pressure distribution become more and more asymmetric, leading to larger and larger sectional side forces. These forces do not change sign in the range of angles of attack investigated here. At $\alpha = 17 \leq$ deg, the side-force coefficient C_y varies only a little along a large portion of the cone, indicating a largely conical flowfield. At higher incidences, deviations from conicality become expressed. This might be attributed to the fact that the tip of a real model has probably some arbitrary, nonconical shape (as was actually verified by examination of various of our cone models under the microscope) and provides arbitrary initial conditions to the flow, which might develop into a conical or nonconical flowfield.[7]

The sectional normal-force coefficient C_n on the basic cone increases roughly linearly with incidence, after asymmetry has set in, as a consequence of the overall effect of the change in vortex strengths and positions of the asymmetric vortices. Again, for $\alpha = 17$ deg almost constant normal-force coefficients are found along the cone, indicating nearly conical flow. With increasing incidence, deviations from conicality become more apparent. The ratio C_y/C_n for the cone without fin starts out with very small values at $\alpha = 15$ deg for nominally symmetrical flow; at the largest measured angle, $\alpha = 35$ deg, the sectional side forces are almost as large as the normal forces ($C_y/C_n \approx 80\%$). The values of the ratio do not show much variation over a large part of the cone, except near the tip; see Fig. 3. When the fin is attached to the cone, we ob-

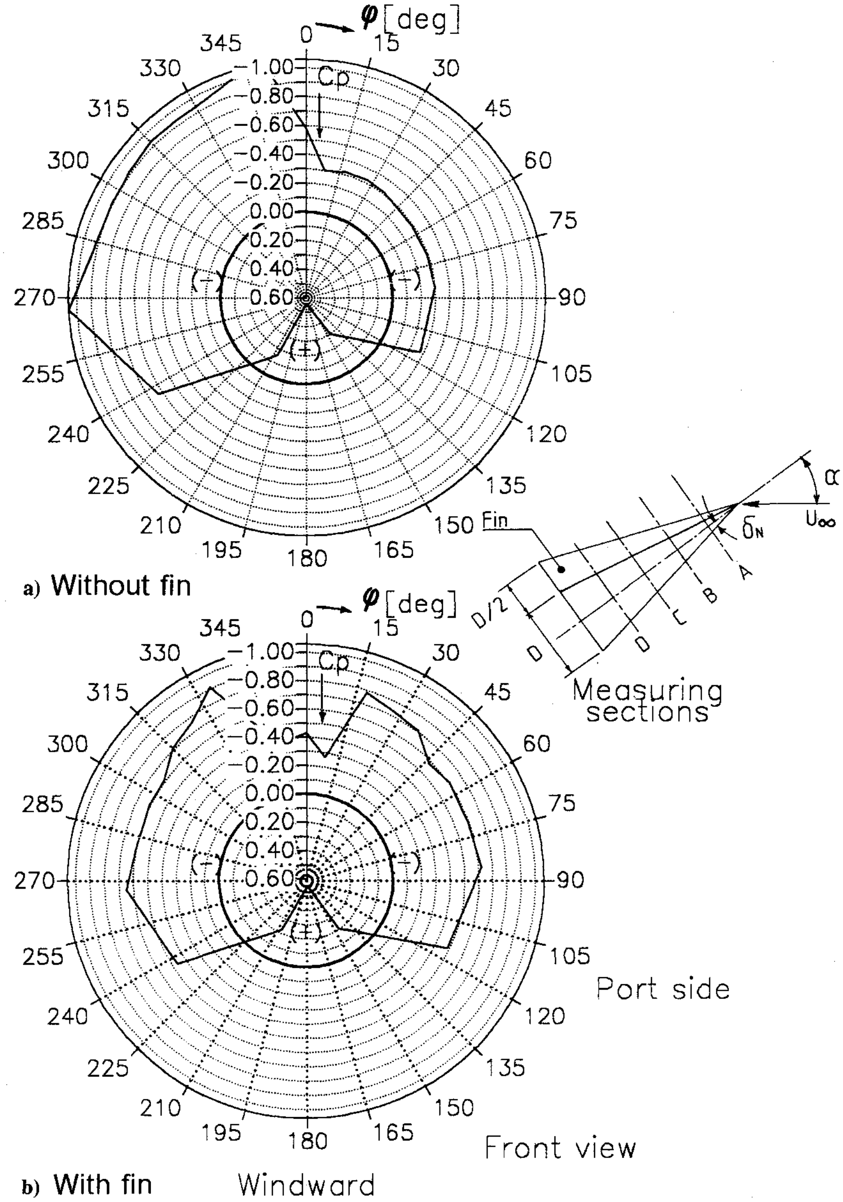

Fig. 2 Circumferential pressure distribution on circular cone without and with fin, at α = 35 deg, and Re_D = 1.42 × 10^5 at section C.

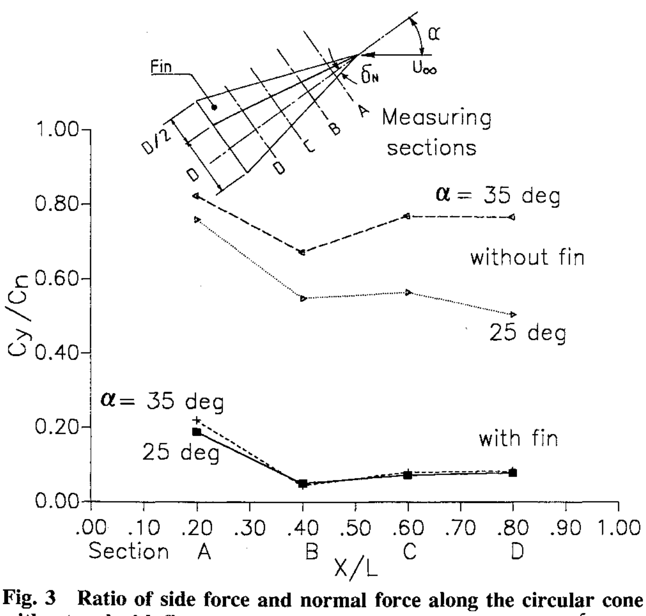

Fig. 3 Ratio of side force and normal force along the circular cone without and with fin, at α = 25 and 35 deg, and Re_D = 1.42 × 10^5.

serve that the sectional side-force coefficients on the cone have dropped by an order of magnitude along most of the cone from the values obtained on the basic cone. It can, therefore, be concluded that the use of such a lee-side fin on a circular cone is quite effective in reducing side forces. The sectional normal-force coefficients on the cone without and with fin attached, on the other hand, differ only slightly. Obviously, in the presence of the fin, the otherwise asymmetric vortex configuration adjusts in such a way that the vortices assume some intermediate, symmetric position and strengths, so that the overall flowfield provides practically the same sectional normal force at each section.

Conclusions

Flow visualization tests carried out on a slender circular cone without and with a fin attached to the lee side demonstrated that the fin largely suppresses vortex-flow asymmetry that is present on the cone without fin. Circumferential pressure measurements at four sections along the cone showed that the fin is reducing the large side forces acting on the cone without the fin by an order of magnitude to very small values. Furthermore, it should be possible to use a vertically movable fin, with height, insufficient to suppress asymmetry, to exploit the associated side force for control purposes.

Acknowledgments

The support of this work by KFUPM, Dhahran, Saudi Arabia, and Deutsche Forschungsanstalt fuer Luft-und Raumfahrt (German Aerospace Research Establishment), Göttingen, Germany, is gratefully acknowledged.

References

[1]Ericsson, L. E., and Reding, J. P., "Asymmetric Flow Separation and Vortex Shedding on Bodies of Revolution," *Tactical Missile Aerodynamics: General Topics*, 2nd ed., edited by M. J. Hemsch, Vol. 141, Progress in Astronautics and Aeronautics, AIAA, Washington, DC, 1992, pp. 391–452.

[2] Prandtl, L., and Tietjens, O., *Applied Hydro- and Aeromechanics*, 1st ed., Dover, New York, 1934, pp. 279, 280.

[3]Foeppl, L., "Wirbelbewegungen hinter einem Kreiszylinder," Sitzungsbericht, Koniglich Bayerische Akademie der Wissenschaften, Math.-Phys. Klasse, Jg. 1913, Munchen, Germany, Jan. 1913.

[4]Stahl, W., "Suppression of Vortex Asymmetry Behind Circular Cones," *AIAA Journal*, Vol. 28, No. 6, 1990, pp. 1138–1140; also AIAA Paper 89-3372, Aug. 1989.

[5]Ng, T. T., "Effect of a Single Strake on the Forebody Vortex Asymmetry," *Journal of Aircraft*, Vol. 27, No. 9, 1990, pp. 844–846.

[6]Stahl, W., Asghar, A., and Mahmood, M., "Suppression of Vortex Asymmetry and Side Force on Circular Cone," DLR-IB 222-93 A 12, Cologne, Germany, April 1993.

[7] Pidd, M., and Smith, J. H. B., "Asymmetric Vortex Flow over Circular Cones," *Vortex Flow Aerodynamics*, AGARD CP-494, July 1991, pp. 18-1–11.

Numerical Implementation of a Modified Liou-Steffen Upwind Scheme

Jack R. Edwards*
North Carolina Agricultural and Technical State University, Greensboro, North Carolina 27411

Introduction

SEVERAL recent efforts[1–3] have focused on the development of upwind schemes for the Euler equations that combine the accuracy of flux-difference splittings[4] in the capturing of shear layers with the robustness and low cost of flux-vector splittings.[5] Perhaps the most popular of these "hybrid" upwind algorithms is the advection upstream splitting method (AUSM) of Liou and Steffen.[2] In this approach, the inviscid flux at a cell interface is split into a convective contribution, which is upwinded in the direction of the flow, and a pressure contribution, which is upwinded based on acoustic considerations. The treatment of the convective portion of the flux allows the AUSM to capture a steady contact discontinuity without excess numerical diffusion. As a result, the AUSM can capture shear layers quite accurately, even with a first-order discretization. Under certain conditions, however, a first-order AUSM discretization will capture a strong normal shock in a non-monotone fashion, effectively precluding the possibility of an accurate higher order extension in the shock region. Nevertheless, the AUSM would appear to be a viable alternative to more "standard" upwind approaches, both in terms of accuracy and efficiency.

As with most flux-vector splitting approaches, different forms for the AUSM interface flux are required for subsonic or supersonic values of the state Mach number. In addition, the evaluation of the convective portion of the interface flux for subsonic situations involves a discontinuous switching between left and right states. Potential users of the approach may be daunted somewhat by this seeming complexity, especially if an implicit formulation based on an exact linearization of the AUSM is needed. In this Note, a particular construction of the AUSM interface flux that does not require if-then-else Fortran logic to account for switches among the various states is presented. Based on this "compact" formulation, two linearizations, one nearly exact within a finite volume framework and the other an approximate, but much simpler, node-based formulation, are also presented. A simple method for "blending in" elements of the more dissipative Van Leer/Hänel flux-splitting scheme,[5] useful for eliminating the non-monotone behavior of the AUSM in the vicinity of a strong normal shock, is also included in the analysis. For reasons of simplicity and compactness, the development that follows considers only first-order interpolations from states i and $i+1$ on either side of the cell interface $i+1/2$ and assumes a two-dimensional flow of a single-component perfect gas. Unless otherwise noted, all quantities relating to metric derivatives, etc., are assumed to be evaluated at the cell interface.

Received Feb. 28, 1994; revision received April 28, 1994; accepted for publication April 30, 1994.

*Research Associate, Department of Mechanical Engineering; currently Assistant Professor, Department of Mechanical and Aerospace Engineering, North Carolina State University, Raleigh, NC 27695. Member AIAA.

Interface Flux Definition

We begin by writing the inviscid flux in the kth generalized-coordinate direction ($k = \xi, \eta$) as the sum of convective and pressure components:

$$F \equiv F^c + F^p = \frac{|\nabla k|}{J} M \tilde{F}^c + \frac{|\nabla k|}{J} p \tilde{F}^p \tag{1}$$

where

$$\tilde{F}^c = \begin{bmatrix} \rho a \\ \rho u a \\ \rho v a \\ H a \end{bmatrix}, \qquad \tilde{F}^p = \begin{bmatrix} 0 \\ \tilde{k}_x \\ \tilde{k}_y \\ 0 \end{bmatrix} \tag{2}$$

$$\tilde{k}_{x,y} = \frac{k_{x,y}}{|\nabla k|} \tag{3}$$

$$H = \rho[\gamma e + (1/2)(u^2 + v^2)] \tag{4}$$

$$p = (\gamma - 1)\rho e \tag{5}$$

The contravariant Mach number M is given as

$$M = \frac{1}{a}(\tilde{k}_x u + \tilde{k}_y v) \tag{6}$$

where a is the speed of sound.

Following Ref. 2, we define an appropriate interface flux $F_{1/2}$ by considering the behavior of the convective and pressure components separately. The convective portion of the interface flux $F^c_{1/2}$ is given by

$$F^c_{1/2} = \frac{|\nabla k|}{J}(C^+ \tilde{F}^c_i + C^- \tilde{F}^c_{i+1}) \tag{7}$$

where

$$C^+ = \alpha_i^+(1.0 + \beta_i)M_i - \gamma^+_{1/2}(1.0 - \delta_{1/2}) \times (\beta_i M_i^+ + \beta_{i+1} M^-_{i+1}) - \delta_{1/2}\beta_i M_i^+ \tag{8}$$

and

$$C^- = \alpha^-_{i+1}(1.0 + \beta_{i+1})M_{i+1} - \gamma^-_{1/2}(1.0 - \delta_{1/2}) \times (\beta_i M_i^+ + \beta_{i+1} M^-_{i+1}) - \delta_{1/2}\beta_{i+1} M^-_{i+1} \tag{9}$$

In the preceding equations, the split Mach number $M^{\pm}$ is defined as

$$M^{\pm}_{i,i+1} = \pm(1/4)(M^{\pm}_{i,i+1} \pm 1.0)^2 \tag{10}$$